General Relativity and Gravitation, Vol. 15, No. 2, 1983

Gravitational Waves and Red Shifts: A Space Experiment for Testing Relativistic Gravity Using Multiple Time-Correlated Radio Signals

L. L. SMARR[1] and R. F. C. VESSOT

Harvard-Smithsonian Center for Astrophysics, Cambridge, Massachusetts 02138

C. A. LUNDQUIST and R. DECHER

NASA Marshall Space Flight Center, Huntsville, Alabama 35812

and

TSVI PIRAN[2]

Racah Institute of Physics, The Hebrew University, Jerusalem, Israel and Institute for Advanced Study, Princeton, New Jersey 08540

Received January 17, 1980; revised December 1981

Abstract

We describe an experimental technique for detecting extremely low-frequency pulses of gravitational radiation ($\nu_{GW} \sim 1$–10 mHz) originating from collapsing supermassive objects ($M \sim 10^6$–$10^7\, M_\odot$) occurring anywhere in the universe. Our technique is the natural outgrowth of a previous gravitational space mission. The novelty of our approach is in placing a highly stable hydrogen maser onboard a deep-space probe that controls a transmitter sending signals to earth. The spacecraft also includes a doppler transponder operating in the conventional two-way mode. Doppler tracking using simultaneously acquired one- and two-way information both on the spacecraft and at the earth station provides four time-records of frequency fluctuations. A single gravitational disturbance manifests itself as a uniquely determined pulse sequence in the two or more data sets whose amplitudes and arrival times depend on a single parameter. The repetition of the signal and the noises in the data can be used in a filtering scheme to improve the amplitude sensitivity by a factor of about 6 in amplitude (36 in energy). We believe the most likely of these gravitational pulse events occurring frequently enough to be detected (more than once per year) will come from the

[1] Junior Fellow, Harvard Society of Fellows. Current address: Department of Astronomy, University of Illinois, Urbana, Illinois 61801.
[2] Revson Fellow, Hebrew University.

0001-7701/83/0200-0129$03.00/0 © 1983 Plenum Publishing Corporation

formation of black holes in the cores of ordinary spiral galaxies. We propose a technologically feasible and realistic space mission, using the above technique, to measure two aspects of gravitation with the same experimental equipment. The spaceflight begins in a highly eccentric earth orbit to measure the gravitational red shift and the second-order doppler effects to an accuracy of 5 parts in 10^6; at this level significant new tests of nonmetric theories of gravity are possible. Later, the spacecraft is sent into a heliocentric orbit to distances beyond 6 AU to search for gravitational radiation.

§(1): *Introduction*

Gravitation is one of the four fundamental interactions in nature, together with electromagnetism, the weak, and the strong forces. There is an elegant theory of this interaction—the general theory of relativity. Yet, the question of whether this theory accurately describes gravity has not been conclusively answered. We suggest herein two very fundamental experiments in gravitational physics carried out by a new space mission that uses the Space Transportation System (Space Shuttle) of the National Aeronautics and Space Administration (NASA). It begins with a near-earth, highly eccentric orbit, to test the gravitational red shift. Later, the spacecraft is placed into a heliocentric orbit to provide a long earth-to-spacecraft baseline that will allow the most sensitive search thus far proposed for bursts of low-frequency gravitational waves from astrophysical sources.

Our paper is divided into four major sections following the Introduction. In Section 2 we discuss the doppler tracking system, common to both experimental objectives. Previous studies have been restricted to simple two-way doppler systems employing transponders only on spacecraft and clocks only on earth. An essential innovation of our experiment is the use of *four* simultaneous sources of doppler tracking phase data between a clock on earth *and* a clock on the spacecraft [1, 2]. We regard this system as the logical next step in precision Doppler tracking.

The use of a clock onboard and the four links will enable us to filter out the Doppler effects of the earth's troposphere and antenna motion, which is the dominant noise source. The effects of the clocks, receiver noises, deep-space propagation anomalies, and spacecraft buffeting, considered as continuous noise processes, are accounted for. Discrete pulses that are large compared to the noise continuum are removed by time-correlation processes. In particular, we point out that a drag compensation system to remove nongravitational accelerations is not required. This doppler system makes possible the correlation and pattern-recognition analysis of one- and two-way Doppler data that will make a very substantial improvement in the detection sensitivity for low-frequency gravitational waves.

We show in Section 3 how the use of this system allows very high-accuracy tests of various interpretations of the equivalence principle, the foundation of

any theory of gravity. We review how electromagnetic signals propagating between material test bodies probe the consistency of relativistic theories. In particular, we use a theoretical framework of Ni's [3, 4] to compare the red-shift experiment with Hughes-Drever and Eötvös experiments. We find that the 1976 suborbital Gravity Probe A [5], a joint Smithsonian Astrophysical Observatory (SAO) and NASA mission, competes very favorably with these other experiments for particular aspects of the equivalence principle at the 10^{-4} level. The Gravity Probe A (GPA) experiment successfully demonstrated the basic techniques of using masers on spacecraft and the multiple Doppler links described in Section 2. Building on this successful test of the equipment, we propose as a first phase of this experimental program to fly an orbital mission, as originally envisioned [6, 7], to improve the red-shift measurement by a factor of 100. A further improvement will result from simultaneous acquisition of data both from the earth station and from the probe, allowing the red-shift and second-order Doppler effects to be identified separately.

If these red-shift test results are consistent with gravity being a metric theory, conceptually we can proceed to the next level, which is to test the static limit of the theory. Here the laboratory for precise measurements is the solar system. Over the last decade, very sensitive measurements of time delay in radio signals passing close to the sun from spacecraft have enabled us to verify the static Einsteinian corrections to Newtonian gravity to better than 10^{-3} [8, 9]. These experiments have eliminated most of the other competition to Einstein's theory of gravitation. Our mission will have the capability to refine these experiments by virtue of its highly accurate tracking and timing capability. Because of the current high precision of these experiments and the well-understood techniques upon which they depend, we will not discuss them further here.

Finally, we arrive at the as yet untested level--that of the dynamical theory. One expects that any theory of gravity incorporating special relativity will predict gravitational waves. A major new area for testing dynamical relativity is the binary pulsar PSR1913+16. As reported by Taylor, Fowler, and McCulloch [10], the system is losing energy very nearly at the rate predicted by general relativity. Most other theories of gravity are ruled out by this new test [9]. This exciting *indirect* evidence for the existence of gravitational radiation heightens the need for the *direct* measurement of the interaction of a gravitational wave with experimental apparatus. In Section 4 we discuss a mission that uses the earth and a distant spacecraft as a free-mass wide-bandwidth detector for directly observing bursts of low-frequency gravitational radiation [11, 12]. The system we describe uses pattern-recognition and time-correlation techniques to determine the actual waveform of the burst and to verify that it is gravitational in origin. The astrophysical process that most likely would cause such bursts is the formation or collision of supermassive black holes anywhere in the observable universe ($z \gtrsim 3$). We show that if such bursts occur as often as once per year, they are likely to originate in the nuclei of ordinary spiral galaxies, such as our own or M31.

We emphasize throughout that we are proposing a realistic space mission, which we see as the logical next step in the space-based study of relativistic gravity. In Section 5 we outline a possible mission profile that would accomplish our objectives.

In summary, to make precise measurements in gravitation, highly accurate clocks and rods are needed. For this reason, our mission will place the best available oscillator onboard the spacecraft as well as on the ground. To guarantee that these "rods" measure only the effects of gravitational fields, we employ the four-link tracking system. To present credible arguments that this proposed mission can accomplish our observational goals, we describe the hardware and detection techniques in detail. With this technology, we can make tests of theories of gravitation at three fundamental levels: the foundations, the static limit, and the dynamical level.

§(2): *Doppler Systems*

Doppler frequency measurements, using continuous-wave microwave signals transmitted to and from spacecraft, provide data for determining the rate of change of range distance. This mode of tracking employs a phase-coherent transponder on the space vehicle to receive a continuous wave signal from the earth station and to retransmit a phase-coherent signal back to earth. In the systems we discuss here, the frequency of this signal is a rational multiple, R_2 (e.g., 240/221), to provide a frequency offset in the retransmitted frequency from that of the signal received at the spacecraft. The phase of the signal received at the ground station is compared with that of a signal generated by the ground transmitter master oscillator, which is also offset by the same ratio, R_2. Counting and recording the beat cycles of the phase comparison as a function of time gives the change of the range distance to the spacecraft over a given time interval and the range rate can thus be calculated. This is the "two-way" mode of operation. If the spacecraft's retransmitted signal is received by a station other than the one transmitting to the spacecraft, the rate of change of the *total* ray path up to the spacecraft and back to the earth station can be determined as a function of time; this is the three-way mode of operation. Normally, simultaneous Doppler measurements using two-way and one or more three-way combinations of widely separated stations are used for the determination of spacecraft orbits to high accuracy. This process is illustrated in the earth–spacecraft–earth signal path shown as "loop A" in the space-time diagram in Fig. 1. The output signal representing the phase comparison of the return signal with the earth station oscillator at a given coordinate time t is shown as $E_2(t)$.

At present, this is the most commonly used method to obtain range-rate information at high accuracy: the range-rate data are fitted to ballistic trajectories by use of sophisticated models of the geopotential and various terms to

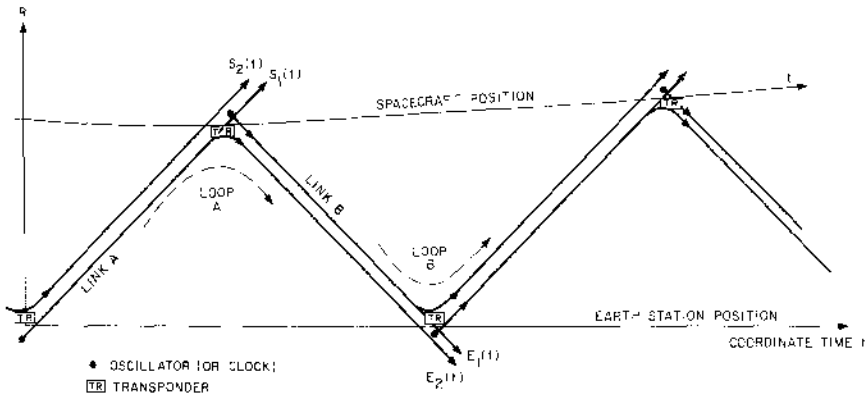


Fig. 1. Space-time diagram of Doppler signals.

account for atmospheric drag, light pressure, vehicle outgassing, etc. In addition, position information can be obtained with the same transmitter-receiver system by modulating the phase of the uplink signal and measuring the round-trip time-lapse for the reception of the modulated signal at the earth station. While in the following discussion our interest is centered on the range-rate determination that operates by recording the phase of microwave signals from the spacecraft, if required, the system can also be operated to recover the modulated signal and obtain range information.

If an oscillator is placed on a space vehicle, we can make one-way measurements of range-rate by comparing the phase of the incoming cycles with a signal generated from a similar oscillator at the earth station. This is shown in Fig. 1 as link B. In a system where both loop A and link B operate together, we can remove first-order Doppler effects of the relative motion of the vehicle and earth station from the one-way signal shown as link B by subtracting one-half of the two-way Doppler cycles from the one-way Doppler cycles accumulated from link B. The remaining Doppler accumulation is the result of the gravity potential difference between the space vehicle and the earth station, the second-order Doppler effect, and the effect of the motion of the earth station during the light time of the signals.

This combination of one-way and two-way signals was used in the 1976 gravitational red-shift experiment (GPA) where a hydrogen maser clock was launched to an altitude of 10,000 km in a suborbital trajectory [5]. The basic hardware for the Doppler system was adapted from the existing Unified S Band (USB) system developed by NASA. The three microwave links were transmitted and received using a single antenna at the earth station and on the space probe; the details of the system are described later.

The success of the simultaneous one-way and two-way Doppler system has led us to propose the next step in the evolution of Doppler systems [1]. Here,

we propose to make the system completely symmetrical by adding an uplink from a transponder at the earth station that retransmits the signal from link B back to the spacecraft. The resulting two-way Doppler system operated at the spacecraft is shown as loop B in Fig. 1. We now have the opportunity to obtain one-way and two-way data *both* at the spacecraft and at the earth station. The arrows indicate the position in coordinate time of the Doppler phase information labeled E_1, E_2, S_1, S_2, that represent the earth station one-way and two-way, and space station one-way and two-way phase data, respectively. As is pointed out in the forthcoming discussion, the phase variation of these links will be shown in coordinate time on four parallel plots to illustrate time correlation of several different aspects of the system's behavior.

Figure 2 is a block diagram of the system. Here, the four signal links are shown physically separated. However, even though they must operate at different frequencies to prevent self-excitation and jamming, the signals can be made to share the same antenna and antenna feed systems and thus any significant geometrical separation between the points of origin and reception of the signals is eliminated. It is important to understand that this system is completely phase-coherent; no cycles of phase are allowed to slip undetected and all frequency multiplications are made with the integer ratios R_i. The high-stability oscillators (or clocks) serve several different functions: as master oscillator for the transmitter, local oscillator for the receiver, and proper clock (as distinct from a coordinate clock) for time synchronization.

Loop A consists of a signal obtained by multiplying the earth oscillator proper frequency f_0, by the ratio R_1, which is transmitted to the spacecraft as link A and then returned to the ground station after frequency multiplication by ratio R_2 in the transponder. The signal is received at the earth station and compared at mixer a with a signal at a frequency $R_1 \times R_2 \times f_0$. This completes loop A. The output beat is designated $E_2(t)$, the two-way Doppler signal. One-way Doppler data are obtained at the spacecraft by comparing the signal frequency from link A with a signal at frequency $R_1 f_0$ at mixer b. This information is telemetered to earth in the form of cycle counts and the *proper* times at which they are accumulated.

As seen in Fig. 2, the system shown in solid lines is completely symmetrical. The spacecraft oscillator-controlled downlink (link B) is part of loop B. The spacecraft two-way signal (S_2) and the earth station one-way signal (E_1) are derived using ratios R_3 and R_4 to obtain the necessary frequency separations. In the red-shift system flown in 1976, the system operated at S band and consisted of loop A and link B. Here the oscillator was an atomic hydrogen maser oscillating at 1,420,405,751.68 Hz and the ratio R_1 was 82/55, which provided an uplink frequency of 2117.7 MHz. The ratio R_2 was the usual Unified S Band transponder ratio 240/221 and the downlink frequency was 2299.8 MHz. The ratio R_3, chosen to minimize the first-order dispersion of the earth's ionosphere, was 76/49 [13], which placed the clock downlink at 2203.1 MHz.

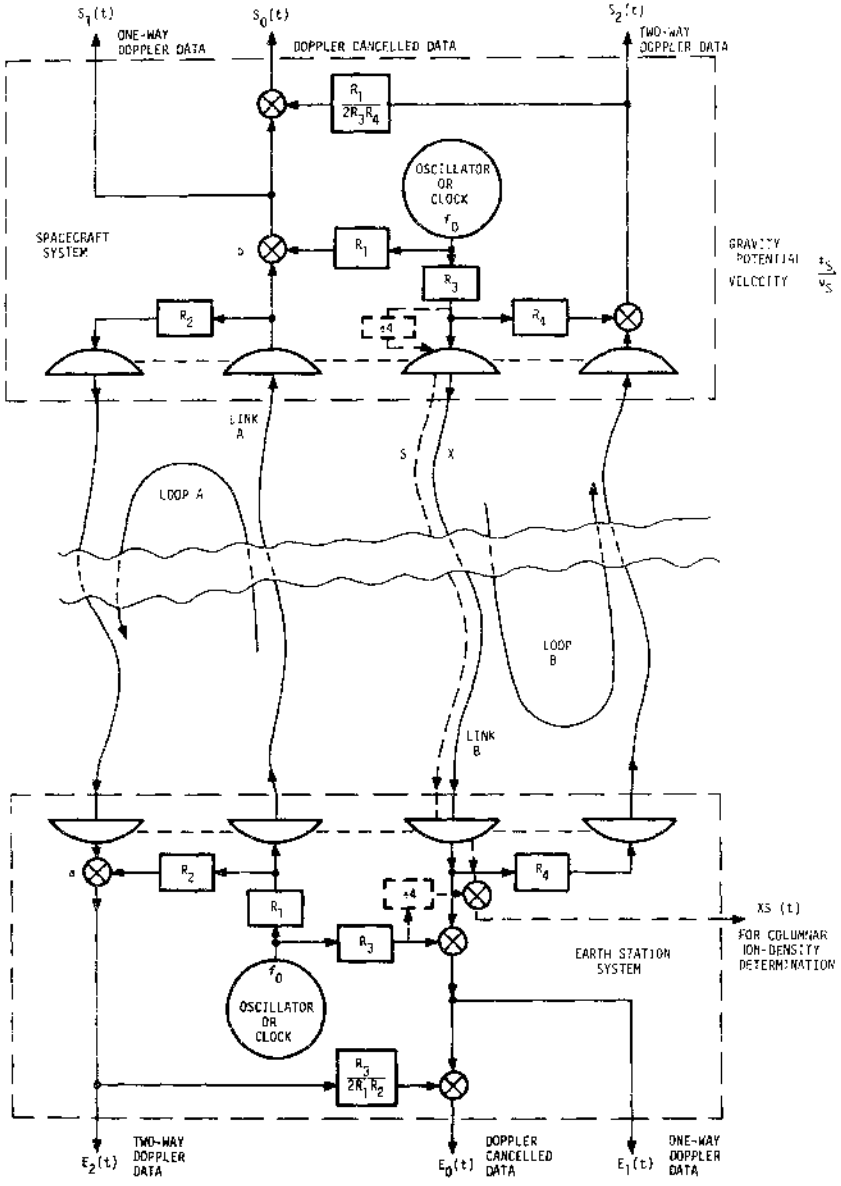


Fig. 2. Concept of four-link time-correlated Doppler system.

The first-order Doppler effects contained in the one-way link can be canceled by subtracting one-half the two-way Doppler phase from the one-way phase accumulation. This produces the Doppler-canceled data labeled E_0 and S_0 in the earth and probe station, respectively. These signals contain gravita-

tional red-shift and relativistic effects due to the motion of the earth and probe. Alternatively, we can combine the one-way earth station data [$E_1(t)$ and $E_2(t)$] and the spacecraft data [$S_1(t)$ and $S_2(t)$] to obtain a redundant data set for $E_0(t)$ and $S_0(t)$. In particular, measurements of the uncanceled one-way phase fluctuations can be obtained in both directions to assess the propagation conditions in the system.

The system shown in Fig. 2 is intended to operate at X band with a single S-band auxiliary link (shown dotted) operating coherently with the X-band link B to allow measurement of the columnar electron density in the ray path for *a posteriori* ionospheric corrections to the data. The columnar density data are also required for correcting the range data to obtain an accurate trajectory determination. This information would also be required if the four links involved a combination of frequencies in different microwave bands. The outputs $E_1(t)$ $XS(t)$ shown in Fig. 2 will provide the necessary information.

We now discuss the use of this system in the two principal experiments for our proposed mission: the gravitational red shift and the search for gravitational waves. In the first, the system compares the rates of the oscillators while the spacecraft is in a near-earth eccentric orbit and the light time is short compared to the rate of time variation of the geopotential between the earth station and the spacecraft. Under these conditions the output signals E_0 and S_0 will provide real-time cancellation of changes in the electromagnetic length of the ray paths that occur slowly compared to the light time.

The second regime of operation requires large distances between the earth and space station where $\tau = R/c$ is long compared to the time intervals characterizing the phenomenon we wish to measure. Under these conditions changes in Doppler rates recorded in the four data sets will provide information that will be later processed by using time-correlation and pattern-recognition techniques.

Because the expected rate of occurrence of gravity waves is low and their magnitudes are small, in the search for gravity wave pulses we must consider all sources of continuous noise and all sources of large, discrete pulses that can lead to false alarms. In this paper we separate these systematic occurrences into four categories:

1. Oscillator phase fluctuations on a time scale short compared to R/c.
2. Discontinuous accelerations of the spacecraft from outgassing or buffeting by the solar wind; near-earth propagation variations owing to tropospheric and ionospheric fluctuations, which are considered as part of the movement of the earth antenna, and are the largest continuous noise source.
3. Deep-space plasma effects causing phase fluctuations of duration short compared to R/c.
4. All dispersive plasma effects in the ray path whose fluctuations are slow compared to R/c.

We now discuss how the four-link system described in Figs. 1 and 2 provides information wherein these effects can be separately identified using time-correlation and pattern-recognition techniques. A more detailed discussion for a particular system configuration is given in Vessot and Levine [1].

(a) Identification of Oscillator Instability. Figure 3 repeats Fig. 1 and includes four separate coordinate time plots representing the phase residuals in each of the four Doppler data sets after the trajectory solution has been completed. As an illustration, we assume that momentary phase advance has occurred in the earth station oscillator at $t = t_0$ and we see the momentary phase retardation in the one-way and two-way earth station Doppler signal. (Note that the oscillator serves both to control the transmitter and to provide a local oscillator reference frequency, which, in these examples, is assumed to be below the carrier frequency.) At $t = t_0 + (R_0/c)$ at the spacecraft, the effect of the shift of the earth transmitter phase advance can be seen. At $t = t_0 + (2R_0/c)$ [3] we see in the earth two-way Doppler trace the phase advance in the transponded signal received at the earth station. These pulses have a characteristic signature pattern in three of the four links. A similar offset of the spacecraft oscillator will cause a corresponding set of variations in the Doppler data if we reverse the identification of the earth and spacecraft Doppler data traces. Pattern-recognition and correlation algorithms can be used to identify these clock-related processes and remove their effects from the data.

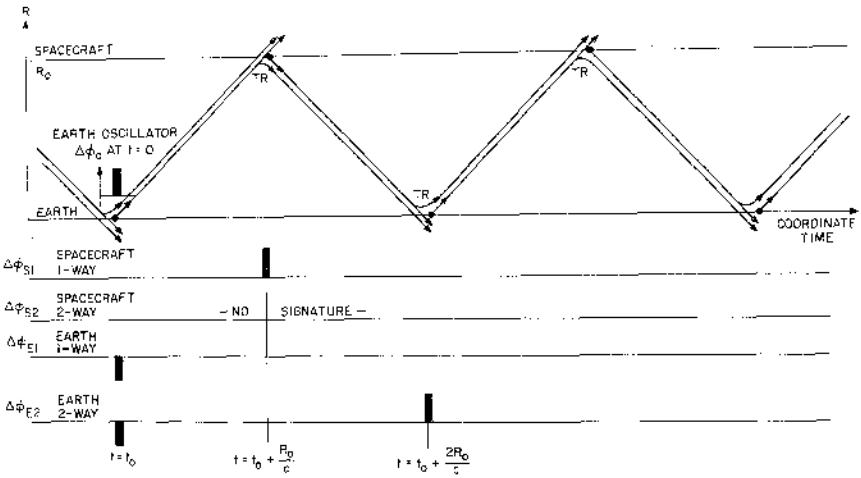


Fig. 3. Effect of momentary phase offset of ground-station oscillator at $t = t_0$ as observed in the four-link correlated system.

[3] In this, and other examples to follow, we assume for simplicity that the range distance is constant and write the two-way light time as $2R_0/c$.

(b) Identification of Antenna Motion. The effects on the four Doppler signals of buffeting of the spacecraft at coordinate time $t = t_0$ by nongravitational forces, such as a blast of the solar wind, impact from a micrometeorite, or a fluctuation in solar radiation pressure, are shown in Fig. 4. The immediate effect is perceived at the spacecraft in the two received signals $S_1(t_0)$ and $S_2(t_0)$. At $t = t_0 + (R_0/c)$ the earth station sees the signature at double amplitude in the two-way link and single amplitude in the one-way link; at $t = t_0 + (2R_0/c)$ the spacecraft again sees the signature on its two-way link. In the case of the earth antenna, both the tropospheric and ionospheric fluctuations can be considered as local to the antenna, and these large effects, in addition to possible antenna motion, will cause a correspondingly distinctive pattern of signatures in the four sets of Doppler data analogous to the ones described above. While it is true that by operating at higher carrier frequencies, such as *X* band and beyond and even to *K* band, we can reduce the level of Doppler fluctuation from space plasma and ionospheric density variations, the effect of the earth's troposphere still remains and, as long as we are restricted to tracking the probe from an earth station, we will have to account for these fluctuations in our search for gravity waves. Of all the continuous sources of spurious Doppler fluctuations, the tropospheric dominates.

(c) Identification of Propagation Anomalies. The propagation path between the spacecraft and earth station may traverse localized regions containing plasma emanating from the sun that cause short-term (here by definition $< R/c$) fluctuations in the Doppler phase. Characteristic signatures of these fluctuations will exist in the Doppler data. Figure 5 illustrates this process, and we will follow

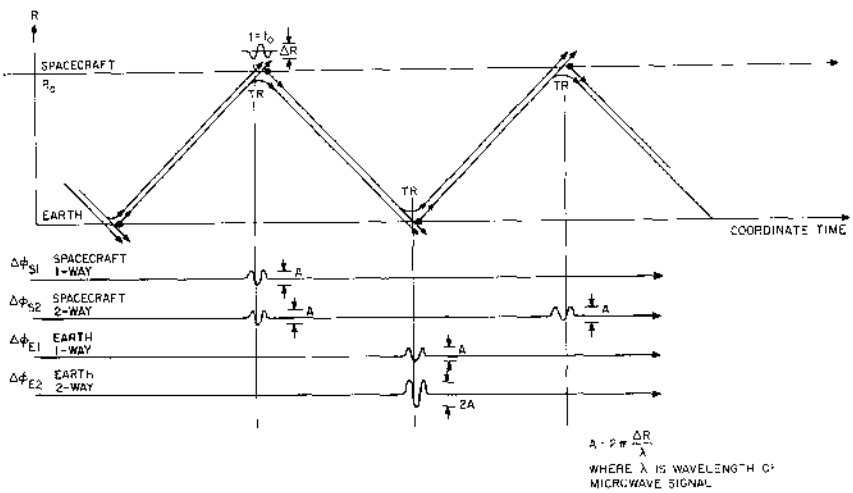


Fig. 4. Effect of spacecraft buffeting.

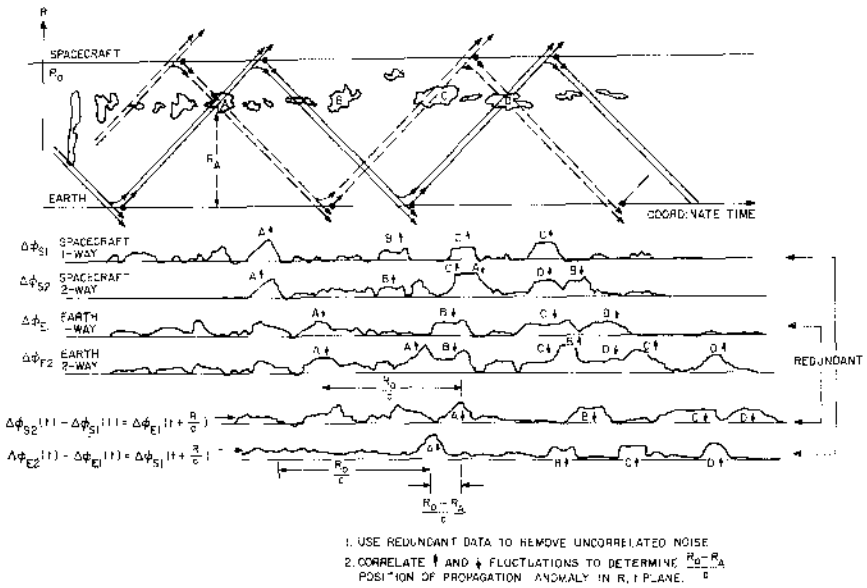


Fig. 5. Illustration of correlation technique to remove effect of phase fluctuations in propagation.

some ray paths to show how the data can be analyzed. We notice that there are two rays passing upward through ionized region A, whose effect is reported in traces S_1 and S_2 at the time marked $A\uparrow$. This example also shows that there are two rays (shown dotted) passing downward through A reported in S_1 and S_2 at time marked $A\downarrow$. In each direction we have twofold redundant information; for example, we have the one-way uplink data reported at S_1 at time $A\uparrow$ and can also obtain a similar representation of this ray path by subtracting the one-way phase data, E_1, from the two-way data, E_2, at the time marked $A\uparrow$ on the E_2 trace. We can thus generate an independent representation of the one-way data at each end of our system, each set of data being obtained by a different set of electronic equipment. By superposition of the redundant one-way data, spaced apart in time by R_0/c, we can reduce the random noise from the electronics and enhance the systematic effects owing to propagation anomalies. We then apply cross-correlation techniques to the upward and downward one-way data with varying time lags to find the position in the ray path at which the ionized "blob" occurred. Figure 5 shows the location of blob A at $R_0 - R_A$ distance from the spacecraft. While it is true that the ray paths upward and downward may not be exactly alike in space-time, we can identify and trace the main features of the disturbances as they cross the ray paths between the earth and spacecraft. The map of these disturbances made from the cross-bearings obtained in space-time will identify the time-varying components of these propagation anomalies whose structures are small compared to R/c. For large-scale variations in the propaga-

tion, which cause fluctuations with time constants R_0/c and slower, we can obtain columnar ion density information using the usual two-frequency data shown from the outputs $XS(t)$ and $S_1(t)$ shown in Fig. 2. (See also [14].)

It is clear that oscillator system and antenna-related disturbances can be easily resolved since their behavior is governed by time lags that are simply related to range distance, R_0. The first steps in data processing will be to search for the patterns shown in Figs. 3 and 4 to identify the location, magnitude, and time of the antenna (including tropospheric and ionospheric effects) and oscillator disturbances.

Localized deep-space propagation anomalies such as those illustrated in Fig. 5 can be removed by a cross-correlation process that will search for patches of ionization that cause phase fluctuations with characteristic times shorter than R/c.

§(3): *Red-Shift Investigation*

We now turn to how this system of Doppler tracking can be used to make measurements of gravitational red shift for testing equivalence principles—the foundations of relativistic gravity theories. We first describe a theoretical framework, then review the results of the successful Gravity Probe A suborbital mission, and, finally, extend these methods to a full orbital mission.

(a) Theory. The red-shift experiment conceptually consists of a comparison of the frequency of the spacecraft clock at various gravitational potentials with respect to a clock at the earth's surface. Comparisons are made using microwave radio signals and, since the spacecraft is in a highly eccentric orbit, substantial first-order and second-order velocity Doppler shifts will accompany the relativistic gravitational potential effect that is to be measured. The fact that the microwave signals are being sent over vast distances means that the comparison of clocks is a very nonlocal process. Furthermore, it is one that relies on the assumption of the isotropy of the *one-way* velocity of light. (For current best experimental limits on the validity of special relativity, see for instance [15]. Our experiment may in fact better some of these limits.) To quantify the data from this rather complex system we usually assume that the clocks, electromagnetic signals, velocities, and gravitational fields are all interacting in the self-consistent manner described by general relativity theory. Any violation we observe would indicate that gravity is a nonmetric theory [9].

However, with the measurement accuracies now available, it would seem prudent to test this consistency to see if Nature acts according to our cherished beliefs. It has proved rather difficult to develop a framework of sufficient generality to allow for all conceivable violations of such fundamental relation-

ships. However, today there are several approaches that can be used to classify nonmetric theories, see, e.g., [9] and references therein.

These approaches are usually phrased as tests of the various equivalence principles of relativistic gravity. The weak equivalence principle (WEP) expressing the universality of free-fall trajectories is tested by the Eötvös experiments. The universality of gravitational red shift (UGR), stating that the red shift is independent of clock structure [16] and the Einstein equivalence principle (EEP), the minimal coupling principle, are tested by red-shift experiments. Schiff, in 1960, argued that the WEP implies the EEP for any complete self-consistent theory of gravity. (See, for instance [17] for a discussion of the above terms.) Lightman and Lee [18] were able to prove Schiff's conjecture for electromagnetically interacting systems in a static spherically symmetric gravitational field (the "TH$\epsilon\mu$ formalism"). Ni [3] later showed that by loosening their assumptions violations of Schiff's conjecture could be found for spinning test bodies. The relationship between the UGR and WEP have also been investigated [16, 19]. Haugan and Will [19] have shown that both the Eötvös experiments and red-shift experiments test possible violations of the WEP (parameters Γ_0 and Λ_0 in the TH$\epsilon\mu$ formalism). It was found that Eötvös experiments give limits of $|\Gamma_0| < 4 \times 10^{-10}$ and $|\Lambda_0| < 6 \times 10^{-6}$. The red-shift experiment tests $-3\Gamma_0 + \Lambda_0$ [9].

Most recently, Ni [4] has investigated what certain aspects of the equivalence principle experiments prove if the implicit assumption that material bodies move on the same metric as electromagnetic fields is removed. Analyzing the Eötvös, Hughes-Drever, and red-shift experiments, Ni finds that the Eötvös and Hughes-Drever experiments demonstrate the equality of the space-space components of the two supposedly different metrics to $\sim 10^{-12}$. However, to get equality of the space-time components, we must divide by $(v/c) \sim 10^{-4}$, where v is the earth's orbital velocity, which leads to tests at levels of 10^{-8}. Finally, he finds the time-time components can be shown to agree only to $\sim 10^{-4}$, since in this instance we must divide by $(v/c)^2$.

This latter accuracy is just at the level tested independently by the 1976 Vessot and Levine GPA experiment [5]. The proposed orbital mission will improve this by 30, placing our confidence in the foundations of the theory on new ground. (For more details on this approach see Ni [4].) Even within the more restricted TH$\epsilon\mu$ formalism, the orbital mission would test Λ_0 at the level 5×10^{-6} currently tested only by the Eötvös experiment. In what follows we will take a less rigorous point of view, aimed primarily at presenting the results of measurement in an as interpretation-free way as possible. Our basic motivation has been and continues to be to make as accurate a measurement of fundamental quantities as technology allows. We hope that this will motivate a more detailed theoretical analysis along the lines outlined above.

We return to our frequency data from the orbiting experiment. Our plan will

be to use our knowledge of the orbit to calculate the expected red-shift effects from the data and see if unexpected residuals occur. The nonrelativistic (or strictly first-order Doppler) effects can be removed by measuring the first-order Doppler shift with a transponder on the spacecraft in the usual range-rate mode and subtracting one-half the two-way Doppler frequency from the one-way signal generated by the spacecraft hydrogen maser clock as discussed in the system described in Fig. 2.

The output fractional frequency shift, $\Delta\nu/\nu$, at the output labeled $E_0(t)$ of the earth station system shown in Fig. 2 is made up of the following relativistic contributions [5]:

$$\left.\frac{\Delta\nu}{\nu}\right|_{earth} = \frac{\phi_s - \phi_e}{c^2} - \frac{|\mathbf{v}_s - \mathbf{v}_e|^2}{2c^2} - \frac{\Delta T_{se}}{c}\,\boldsymbol{\epsilon}_{se}\cdot\boldsymbol{\alpha}_e + \text{terms of order } c^{-3} \qquad (1)$$

The first term is the difference in the Newtonian gravitational potential, ϕ, between the probe and the earth divided by c^2 (where c is the velocity of light). This is the gravitational effect to be measured. In this measurement the potential is determined from our knowledge of the spacecraft's position with respect to the earth.

The second term is the second-order Doppler shift of special relativity and is proportional to the square of the relative velocity of the spacecraft and earth station divided by $2c^2$. This term can be accounted for by our knowledge of the relative velocity of the earth station and spacecraft at any time.

The third term results from the fact that the station is located on the rotating earth and has centripetal acceleration, $\boldsymbol{\alpha}_e$, with respect to an initial frame chosen here to be geocentric with axes aimed at the "fixed stars." During the one-way light time, $\Delta T_{se} = R/c$, the component of velocity along the spacecraft-to-station unit vector, $\boldsymbol{\epsilon}_{se}$, changes by $(\Delta T_{se}/c)\,\boldsymbol{\epsilon}_{se}\cdot\boldsymbol{\alpha}_e$, giving the fractional Doppler frequency shift shown in the third term of equation (1).

The situation wherein data are obtained aboard the spacecraft is described in equation (2). The sign of the first term is reversed, the second term is unchanged, and in the third term, we see the effect of the acceleration of the satellite during the light time of the earth-to-probe signal:

$$\left.\frac{\Delta\nu}{\nu}\right|_{spacecraft} = \frac{\phi_e - \phi_s}{c^2} - \frac{|\mathbf{v}_e - \mathbf{v}_s|^2}{2c^2} - \frac{\Delta T_{es}}{c}\,\boldsymbol{\epsilon}_{es}\cdot\boldsymbol{\alpha}_s \qquad (2)$$

Equations (1) and (2) allow us to separate the effects of the gravitational potential and the motion of the spacecraft and earth station in the following way [20]. We can parametrize the individual contributions of the three terms in equations (1) and (2) by multiplying the gravitational term by A, multiplying the second-order doppler term by B, and multiplying the third term, which depends on the validity of our inertial frame, by C. Adding equations (1) and

(2), we have

$$\left.\frac{\Delta\nu}{\nu}\right|_{\text{earth}} + \left.\frac{\Delta\nu}{\nu}\right|_{\text{spacecraft}} = -\frac{B|\mathbf{v}_s - \mathbf{v}_e|^2}{c^2} - C\frac{\Delta T_{se}}{c}\epsilon_{se}\cdot[\alpha_e + \alpha_s] \qquad (3a)$$

Subtracting

$$\left.\frac{\Delta\nu}{\nu}\right|_{\text{earth}} - \left.\frac{\Delta\nu}{\nu}\right|_{\text{spacecraft}} = 2A\frac{(\phi_s - \phi_e)}{c^2} - C\frac{\Delta T_{se}}{c}\epsilon_{se}\cdot[\alpha_e - \alpha_s] \qquad (3b)$$

Since the red-shift and second-order Doppler contributions are of comparable magnitude, the two can be measured with similar levels of accuracy.

(b) The Previous Mission. The 1976 experiment was a suborbital rocket flight which described a nearly straight up-down trajectory [5]. The system's performance is shown in Fig. 6, where the residual phase at 2.1177 GHz is plotted versus time. This is the result of taking the output E_0 of Fig. 2 and subtracting a phase prediction from equation (1) based on trajectory data and corrections from telemetry. The slopes of the observed and predicted phase are matched over a 10-min interval at apogee and this slope correction is used as the normalization of the spacecraft and earth clock frequency throughout the whole data set.

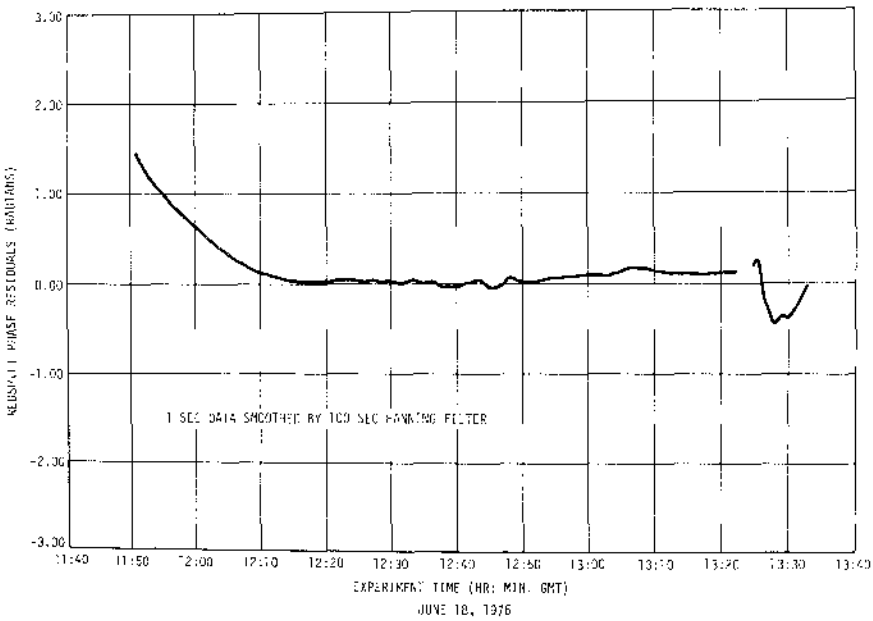


Fig. 6. Red-shift phase residuals.

The ground station uplink transmitter suffered a 2-min interruption at 13:22:47 GMT and the data following this time have not been used. Analysis of the time derivative of the data starting at 12:15 when the after-launch transient had died out and ending at 13:22, the time of the uplink failure, gives an average frequency residue of less than 2×10^{-14}. The conclusion is that the test confirms the equivalence principle at the 1.4×10^{-4} level assuming that special relativity is valid. The confirmation of the combined effects of special relativity and the equivalence principle is at the 0.7×10^{-4} level [21].

The effectiveness of the Doppler cancellation system in removing propagation related fluctuation is shown in Fig. 7, which shows the comparison of the

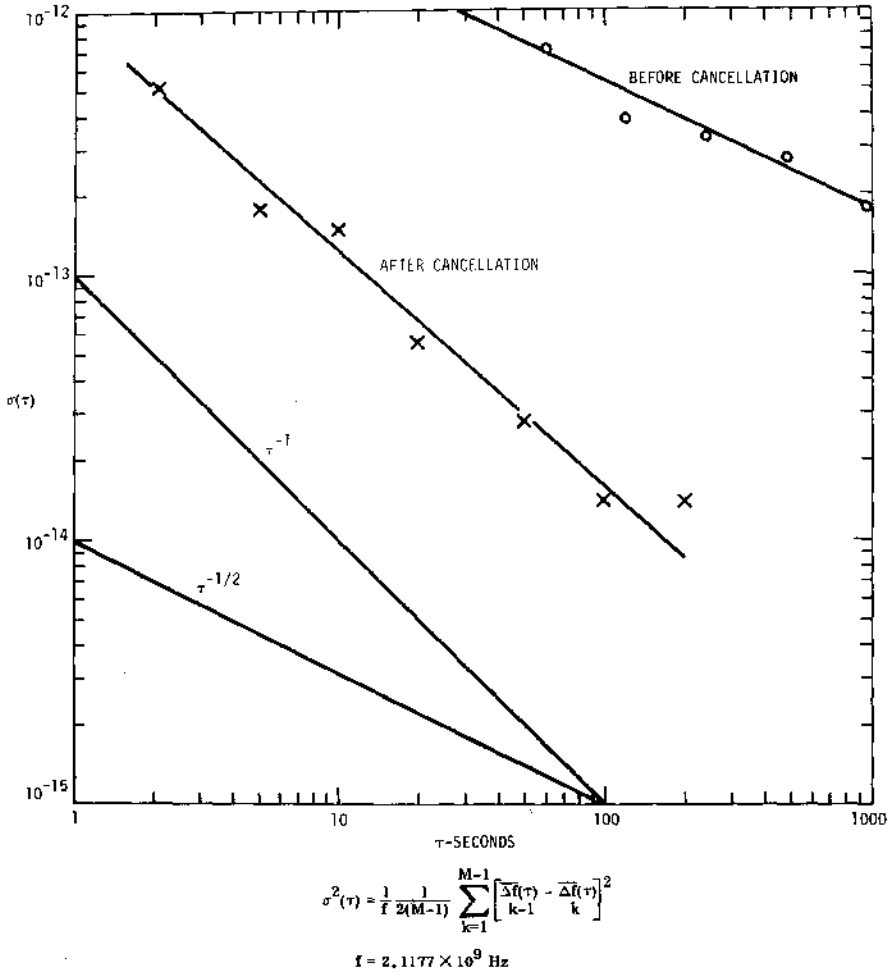


Fig. 7. Allan variance of one-way frequency residuals before and after application of Doppler cancellation system.

one-way Doppler fluctuations and the canceled Doppler fluctuations from the $E_0(t)$ output in the system as represented by the Allan variance [22]. The Doppler-canceled data replicate very closely the results obtained by making maser comparison in the laboratory, indicating that the disturbances that existed in the three ray paths were very nearly canceled and that the effectiveness of the correlation process was not limited by the electronics. A detailed description of the electronics system is reported elsewhere [23].

(c) The Proposed Mission. The system for the eccentric orbit phase of the suggested mission differs from the system originally proposed in 1970 for a satellite experiment [6] in that it is made completely symmetrical by providing a fourth microwave link transponded from earth to the spacecraft as shown in Fig. 2. Now both the spacecraft and the earth station obtain Doppler-canceled data as well as one-way and two-way data.

From the data now at hand from the 1976 rocket probe test, we see that the principal source of uncertainty resulted from the two-minute uplink transmitter dropout and the systematic disturbances that ensued, rather than random noise processes. The microwave system and propagation effects contributed little noise compared to the underlying noise of the clocks. More recent results from continuing hydrogen maser developments at SAO are shown in Fig. 8. These data

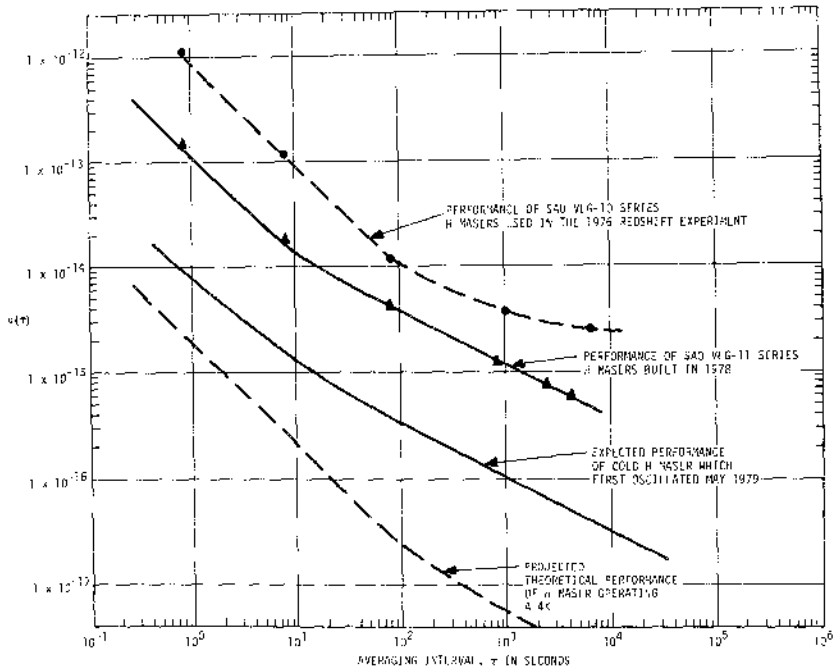


Fig. 8. Performance of hydrogen masers.

are considerably better than those available from the 1976 clocks as can be seen from the same diagram. Also shown in the figure is the stability expected from a cryogenic maser oscillator [24], which was recently successfully operated at 25 K. The lower dotted line shows the expected stability projected for operation at 4 K.

While the accuracy of the test will be improved statistically by the square root of the number of apogee-perigee passes over which data are taken, the ultimate accuracy will depend on our ability to remove systematic effects either by calibration with respect to measurable but uncontrolled variable parameters or by our ability to reduce the effects of such parameters by engineering design. Judging from our present knowledge of the system and its capabilities as summarized in Tables I and II we should be able to attain an accuracy of 5×10^{-6}

Table I. Comparison of Error Budget of Proposed Orbiting Red-Shift Measurement and 1976 Probe Experiment

	1976 Probe operating at 2 GHz (2 hr)	Proposed orbital test operating at 10 GHz (18–24 hr)
Random noise		
Overall microwave system noise including maser instability	13.0×10^{-15}	(4)
Uncanceled atmospheric noise	2.5×10^{-15}	2.5×10^{-15}
Uncanceled ionospheric noise	5.0×10^{-15}	0.2×10^{-15}
Root sum squares (RSS) $\Delta f_r/f =$	14.2×10^{-15}	3.2×10^{-15}
Possible systematic bias errors		
Ground clocks (1σ estimate from variance data made over indicated time interval)	3.0×10^{-15} (for 2 hr)	1.0×10^{-15} (for 18 hr)
Space clock (RSS of all known systematic calibration errors)	4.5×10^{-15}	1.0×10^{-15}
Red-shift and second-order Doppler prediction errors from uncertainties in position and velocity	3.3×10^{-15}	1.0×10^{-15}
RSS $\Delta f_s/f =$	7.9×10^{-15}	1.7×10^{-15}
Combined random and systematic errors in RSS		
RSS $\Delta f_e/f =$	15.5×10^{-15}	4.7×10^{-15}
Variation of $(\Delta\phi/c^2)$ over useful data	1.1×10^{-10}	4.8×10^{-10}
Predicted error in a single red-shift measurement		
$\epsilon = \dfrac{\Delta f_e/f}{\Delta\phi/c^2} =$	141×10^{-6}	9.9×10^{-6}

(4) For 18 hr averages the random noise is $< 1 \times 10^{-16}$. The chief error is systematic and included in the bias contribution.

Table II. Summary of Accuracy for 1976 Probe Experiment and an Estimate of the Accuracy of the Proposed Experiment

	1976 Probe (2 hr)
Formal error from least-squares fit of data to prediction	$\left.\frac{\Delta f}{f}\right\vert = [1 \pm (2.5 \pm 63) \times 10^{-6}] \left[\frac{\Delta\phi}{c^2} + \frac{v^2}{2c^2} + \cdots\right]$
Possible error contribution from systematic effects	$\frac{\Delta f}{f} = \left(\pm\frac{\Delta f_s/f}{\Delta\phi/c^2}\right)\frac{\Delta\phi}{c^2}$ $= \pm 62 \times 10^{-6}\,\frac{\Delta\phi}{c^2}$
Combining as RSS	$\frac{\Delta f}{f} = [1 \pm (5 \pm 140) \times 10^{-6}]\,\frac{\Delta\phi}{c^2}$
	Final result

	Proposed orbital measurement (18–24 hr orbit)
Random frequency error after 30 orbits	$\frac{\Delta f_n}{f} = \frac{3.2 \times 10^{-15}}{\sqrt{30}} = 5.8 \times 10^{-16}$
Random error in red-shift measurement	$\frac{\Delta f_n/f}{\Delta\phi/c^2} = \frac{5.8 \times 10^{-16}}{4.8 \times 10^{-10}} = 1.2 \times 10^{-6}$
Systematic error in red-shift measurement	$\frac{(\Delta f/f)_s}{\Delta\phi/c^2} = \frac{1.7 \times 10^{-15}}{4.8 \times 10^{-10}} = 3.6 \times 10^{-6}$
Predicted sensitivity combining random and systematic effects as RSS	$\frac{\Delta f/f}{\Delta\phi/c^2} = 3.8 \times 10^{-6}$

in the gravitational red-shift measurement and in the measurement of the second-order Doppler effect.

§ (4): *Gravitational Radiation*

Like electromagnetic radiation, gravitational radiation can be caused by transient sources (producing bursts), periodic sources (producing lines), and stochastic sources (producing noise). The known periodic sources are too weak to be seen with the currently planned experiments [25, 26]. Whether stochastic sources can be detected and unequivocally shown to be gravitational radiation is not yet clear [12, 26, 27]. We will not pursue either of these possibilities here and restrict our discussion to the detection of bursts of gravitational radiation.

A gravitational wave burst can be characterized by its dimensionless amplitude $h(t)$. By "burst" we mean the envelope of a waveform that damps out on a timescale $\sim 1/\nu$, where ν is the frequency of oscillation. If we assume that this burst comes from an astrophysical source of mass M and distance from earth r, then the amplitude h is proportional to $\eta^{1/2}\ (M/r)$, where η is the efficiency with which the source converts its mass-energy into gravitational radiation.

Figure 9 shows the best current estimates [25, 28] of the upper limits for astrophysical burst sources. We have assumed we must look out to a distance r, so that the observed volume of space ($\sim r^3$) contains sufficient sources at the given frequency ($\nu \sim M^{-1}$) to give one event per year. These distances range from ~20 Mpc (the Virgo cluster of galaxies) for supernovae (1-10 $M_\odot$) to ~2,000 Mpc (the quasar era) for supermassive (10^5-10^8 $M_\odot$) black holes forming in galactic nuclei.

In Fig. 9 we describe the effects of gravitational waves in what would be considered a very low-frequency region for electromagnetic waves. This means that over the low-frequency, long-wavelength portion of the gravitational wave spectrum ($\nu < 10^3$ Hz or $\lambda_{GW} > 300$ km) detection naturally can be expected to be done over commensurately long distances in space. For the higher end ($\nu > 1$ Hz) of this spectrum, detection can be attempted from earth. In either case, the amplitude of the signal h gives the fractional change in the length R or frequency ν of a gravitational wave detector.

In the figure, the one-sigma background noise level is given for two types of detector systems: (1) the ground-based resonant and free-mass antennas and (2) spacecraft Doppler tracking, specifically, the projected NASA International Solar Polar and Galileo missions and the mission proposed herein. The regions labeled "current sensitivities" are adapted [29] from Weiss [26], and include the recent results from data taken during the Voyager I spacecraft mission. Note that today we are several orders of magnitude away from the conservatively estimated "Black Hole Upper Limit" curves in both regimes.

Even though technology applicable to detecting gravitational waves is progressing rapidly, our estimate of where we will be in the near future is very rough. In Fig. 9 we attempt to estimate from current technology the levels that can be reached in the next few decades. The regions labeled "projected sensitivities" are not limited by fundamental processes; they are extrapolations of existing technological advances. These advances include the use of cryogenic techniques in bar detectors and in hydrogen maser oscillators and superconducting cavity-controlled oscillators.

Further extrapolation of sensitivities into the future can be envisioned that should allow eventual coverage of the entire region considered in Fig. 9. In the high-frequency regime, quantum limits, in principle, can be circumvented for the resonant detectors [30]. For midrange frequencies, space laser interferometers in earth orbit seem possible [26]. In the low-frequency region, much smaller amplitudes would be observed with spacecraft Doppler tracking if phase-coherent

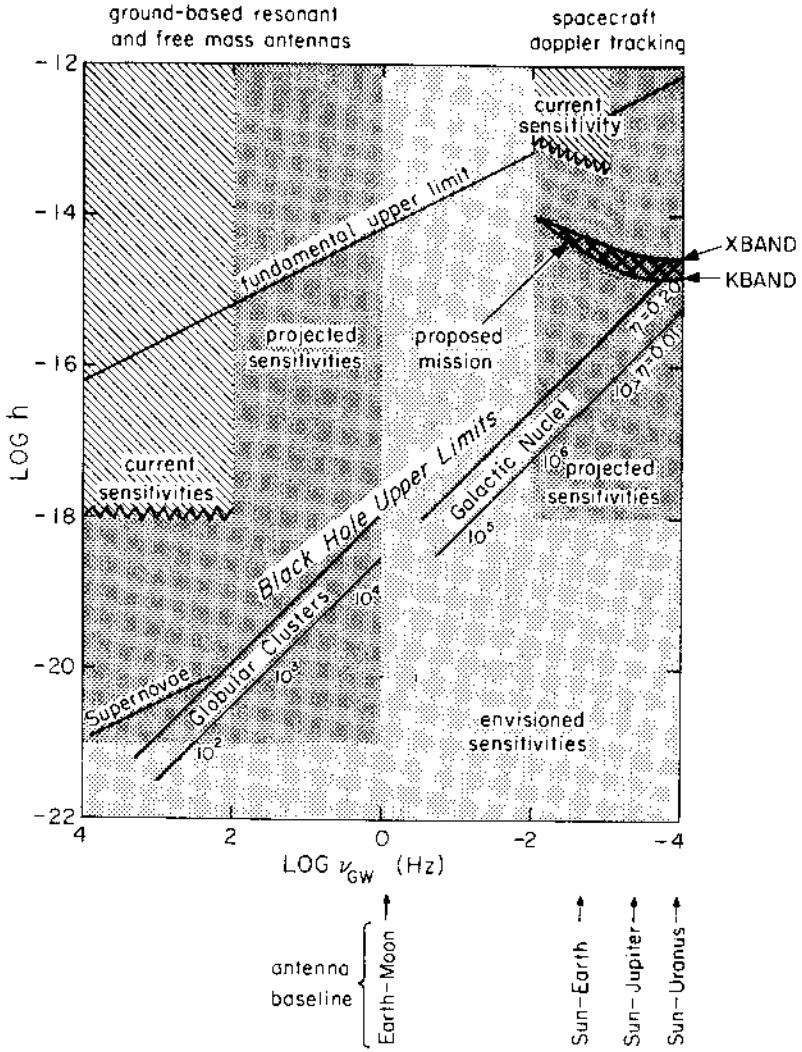


Fig. 9. Amplitude h vs frequency ν_{GW} of gravitational radiation and estimated sensitivity of detectors. The numbers below the black hole upper limits refer to the mass of the source in solar masses.

laser signals were used for tracking between widely separated spacecraft in place of microwave signals.

We see from the rate of progress anticipated in Fig. 9 that the era of gravitational wave astronomy is rapidly nearing. The overlap of the sensitivity of experimental techniques and expected magnitudes of signals from astrophysical sources guarantees exciting new science in the decades ahead.

The heavily cross-hatched region labeled "proposed mission" in Fig. 9 shows the background noise level of the proposed detection scheme after applying the optimum filter [31]. This noise is the superposition of several continuous noise processes. The principal disturbances from the troposphere and the ionosphere have been almost entirely removed by the time-correlated filtering scheme. A separate paper [31] discusses the detection of pulses of gravitational origin. The mission we propose is the most sensitive of the low-frequency gravitational wave experiments currently possible with available technology. It uses microwave Doppler tracking between precision clocks on the earth and on the distant spacecraft. Previous studies [27, 32] have considered how such gravitational waves might appear in two-way Doppler tracking (no clock on spacecraft). Here we will discuss how these bursts appear in the time-correlated, four-link system (clock on spacecraft, described in Section 2), and outline the techniques for identifying them in the presence of noise. Following this, we discuss the amplitude and event rate for possible sources of such burst radiation.

The Doppler signature resulting from a gravitational wavefront intersecting a ray path between earth and a distant spacecraft depends on the mode of observation (that is, whether one-way or two-way), the angle of intersection of the wavefront, and the nature of the originating gravitational disturbance [12].[5]

The one-way signals from space to earth, shown as E_2 in Fig. 2, contain two gravitational wave signatures [34] related in time and magnitude by the parameter $\mu = \mathbf{k} \cdot \boldsymbol{\epsilon}_{se}$, where $\mathbf{k}$ is the wave propagation vector and $\boldsymbol{\epsilon}_{se}$ is the direction of the space-to-earth ray. At the earth station the Doppler frequency shift caused by the wave is given by

$$\left.\frac{\Delta\nu(t)}{\nu}\right|_{\text{one-way } E} = -\frac{(1-\mu)}{2} h_{RE} + \frac{(1-\mu)}{2} h_{TE} \tag{4}$$

where h_{RE} and h_{TE} are the dimensionless wave amplitudes $h(t)$ evaluated at the time of reception on earth and time of transmission of the spacecraft;

$$h_{RE} = h(t_{RE}) \quad \text{and} \quad h_{TE} = h[t_{RE} - (1+\mu) R_0/c]$$

The one-way signals from earth to space shown as S_1 have a similar structure, the sign of μ being reversed. Here

$$\left.\frac{\Delta\nu(t)}{\nu}\right|_{\text{one-way } S} = -\frac{(1+\mu)}{2} h_{RS} + \frac{(1+\mu)}{2} h_{TE} \tag{5}$$

$$h_{RS} = h(t_{RS}), \quad \text{and} \quad h_{TS} = h[t_{RS} - (1-\mu) R_0/c]$$

[5] We will assume throughout our discussion that the wavelength of the gravitational wave is short ($\lambda < R_0/3$) compared to the earth-spacecraft separation R_0. For the inverse case see [26, 33].

These two one-way (TOW) time series of data can be coordinated using appropriate relativistic corrections to bring t_{RE} and t_{RS} into synchronization ane processed using time correlation to remove the major noises and enhance the wave signature.

The time series of data E_2 and S_2 in Fig. 2 also contain wave signatures

$$\left.\frac{\Delta\nu}{\nu}\right|_{\text{two-way } E} = -h_{RE}\frac{(1-\mu)}{2} - h_{TS}\mu + h_{EE}\frac{(1+\mu)}{2} \tag{6}$$

Here

$$h_{RE} = h(t_{RE}), \qquad h_{TS} = h[t_{RE} - (1+\mu)R_0/c]$$

and

$$h_{EE} = h\left(t_{RE} - \frac{2R_0}{c}\right)$$

are the values of $h(t)$ at the following times and places: h_{RE}, time of reception at earth; h_{TS}, the time of signal transponding at the spacecraft; and h_{EE}, the time of signal transmission from earth.

In a similar manner, the spacecraft signal will contain signatures given by

$$\left.\frac{\Delta\nu}{\nu}\right|_{\text{two-way } S} = -h_{RS}\frac{(1+\mu)}{2} + h_{TS}\mu + h_{SS}\frac{(1-\mu)}{2} \tag{7}$$

where h_{RS} is the value of the wave amplitude at the time of signal reception,

$$h_{TE} = h[t_{RS} - (1-\mu)R_0/c] \quad \text{and} \quad h_{SS} = h\left(t_{RS} - \frac{2R_0}{c}\right)$$

The primary gravitational information is in the two one-way channels and occurs there in the form of four pulses. A separate means of obtaining the two one-way data sets is to subtract, in real time, the one-way signal from the two-way signals. For example, if we subtract $E_1(t)$ from $E_2(t)$, we obtain $S_1(t - R_0/c)$. Similarly $S_2(t) - S_1(t) = E_1(t - R_0/c)$. The two pairs of one-way data involve different electronics paths and provide a valuable means for testing the consistency of the results. Alternatively, this method will allow us to obtain information under conditions where it may not be possible or desirable to detect and record one-way phase data aboard the spacecraft for telemetry to earth.

The special temporal structure of the signals and noise in the two one-way data allow us to filter out a large part of the dominant continuous noise by adding and subtracting the data at appropriate times. This process gives significant enhancement of the signal-to-noise ratio of the pulses and can be fine-tuned depending on the structure of the noises. A separate paper describes this process [31].

The improvement using the optimum filter with the two-one-way system is possible if a single, strong (say, 10 times the other noise levels) noise source is present. Table III shows the noise contributions in a presently realizable X-band tracking system given in terms of fractional frequency fluctuations for various time intervals. We have allowed for a high level of ionospheric and tropospheric noise to allow for a wide range of conditions. The bottom line shows the result of optimal time-correlated filtering [31] in the TOW data. The effectiveness depends on the parameter μ of equations (4) and (5). By going from 8.8 to 15 GHz the interplanetary plasma can be further reduced and larger periods of time can be made available with the probe in a generally antisolar direction as discussed by Armstrong [14] and later by Hellings [35].

From equations (4)–(7), it is clear that the probability of detection of a passing burst depends on three factors: the strength of the bursts h, the angle of incidence θ, and the earth-spacecraft distance R_0. Considering a wave of fixed amplitude h in Figs. 10-12, we show how the other two factors (θ, R_0) affect the Doppler frequency signature of the four-link system. If the gravitational wave is propagating within a small angle (e.g., $\theta \lesssim 30^\circ$, Fig. 12) of the earth-probe direction, the pulses merge in a destructive fashion. If the angle θ is fairly large ($\theta \sim 60^\circ$, Fig. 10), a clean separation occurs producing 10 pulses if the envelope of the burst is short ($\sim 1/3$) compared to R_0. Finally, if the propagation is at right angles ($\theta \sim 90^\circ$, Fig. 11) to the earth-probe direction, then each link will have only two pulses (for a total of eight). In addition to this angle dependence, the sensitivity for a given pulse will depend on the projection of the polarization of the pulse on the line joining the earth and the spacecraft.

Table III. $(\Delta\nu/\nu)$ (τ) Frequency Noise–Units of 10^{-15}

	Averaging interval τ (sec)			
Noise contribution	50	100	250	500
H masers [24] (each)	4.2	3	1.9	1.3
TROPO and IONO [23][a] (each direction)	100	100	100	100
Interplanetary [14] scintillation (each direction)	2.7	2.7	2.7	2.7
Probe buffeting [32]	1.5	1.5	1.5	1.5
Earth receiver[b] signal to noise in a 1-Hz noise bandwidth	10	2.5	2.0	1.0
Resulting noise [31] after filtering [depends on μsec equations (4) and (5)]	10.1–11.6	6.8–7.9	4.6–5.3	3.9–4.5

[a] This level should account for a wide range of tropospheric conditions.
[b] Based on existing NASA Jet Propulsion Laboratory Deep Space System at X Band. Earth antenna diameter, 26 m; earth receiver noise temperature, 30 K; uplink power, 50 kW; space antenna diameter, 1 m; spacecraft transmitter power, 2 W.

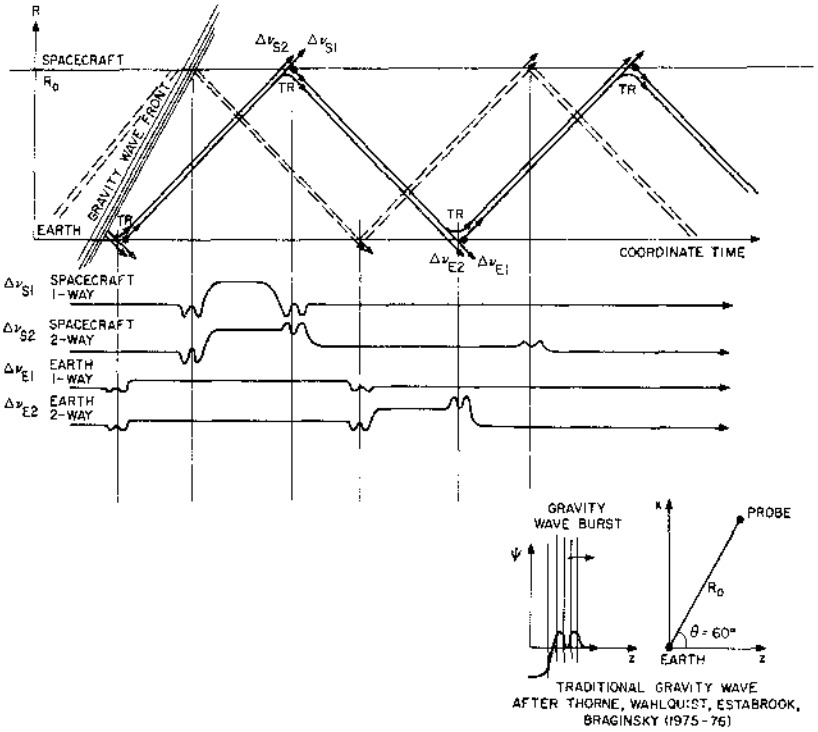


Fig. 10. Illustration of gravity-wave signature for a four-link correlated system, $\theta = 60°$.

We identified in Section 2 three major sources of systematic phase variations in the proposed four-link scheme, which relate to the clock, the antenna, and the propagation paths. We now discuss their importance for the detection of gravitational waves. Since the transmitter and local oscillator are phase-locked to the maser oscillator, the outputs from these systems very closely replicate the performance of the maser oscillator. The antennas and their feed systems are subject to phase variations from thermal effects and mechanical motion. For the very long light times proposed between space and earth systems, the earth's troposphere and ionosphere will be considered an extension of the earth antenna. Tropospheric fluctuations, in particular, are assumed to dominate and, as shown in Fig. 7, can cause fluctuations well into the 10^{-13} level in $\Delta f/f$ at 1000-sec averaging intervals. The successful removal of these effects to the level of the maser stability was done in 1976 using an *S*-band system. We see no fundamental or technological reason not to expect this process to work at the 10^{-15} level or better at 1000-sec averaging time.

Doppler phase variations from changes in the refractive index of signal paths in deep space are overwhelmingly the result of ionization. In principle this source of Doppler phase noise can be overcome by raising the carrier frequency.

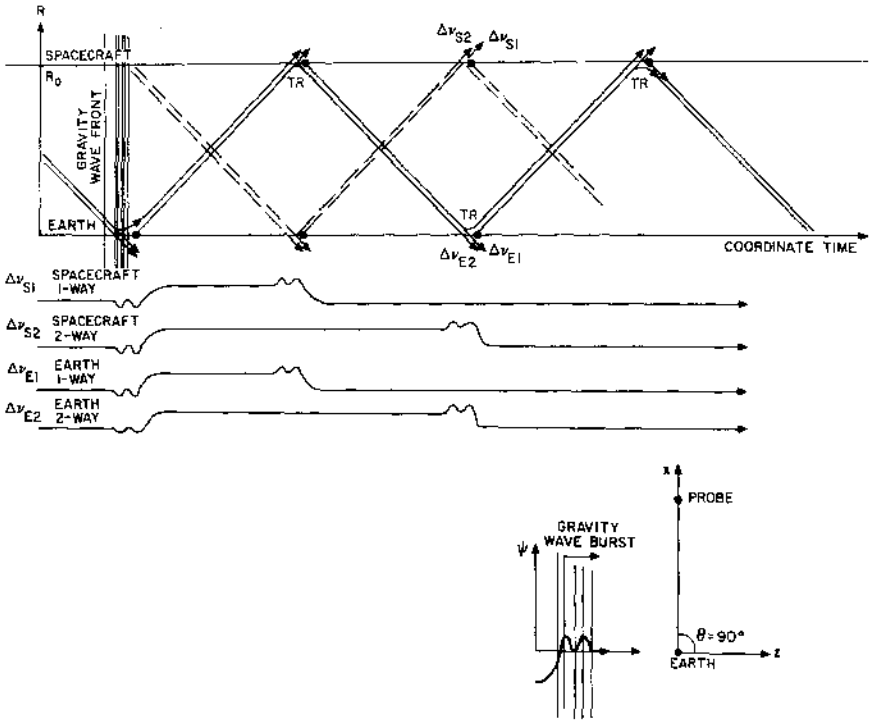


Fig. 11. Illustration of gravity-wave signature for a four-link correlated system, $\theta = 90°$.

In this instance, where we proposed using X-band signals, there can still occur perceptible ionization effects even in ray paths directed well away from the sun. We can measure the average value of the columnar ion density by the usual two-frequency technique using outputs $E_1(t)$ and $XS(t)$ in Fig. 2.

We turn now to a more detailed discussion of the sources of bursts of gravitational radiation in Fig. 9, adapted from Epstein and Clark [25]. The "fundamental upper limit" [25, 36] results from turning galaxies completely into gravitational radiation in a Hubble time. Below this line and above our black hole upper-limit line could lurk unsuspected sources of bursts. We note that gravitational wave detectors with "current sensitivities" are now well below this limit in both the high- and low-frequency regimes.

We have plotted what we believe to be a conservative "black hole upper limit" in Fig. 9. This is the level at which we could begin to observe known or speculated astrophysical objects. At the high-frequency end of this upper limit are core collapses in supernovae in the Virgo cluster ($r \sim 15$ Mpc). At this distance a burst rate of greater than one per year is expected. The efficiencies of gravitational waves from supernovae forming either neutron stars or black holes

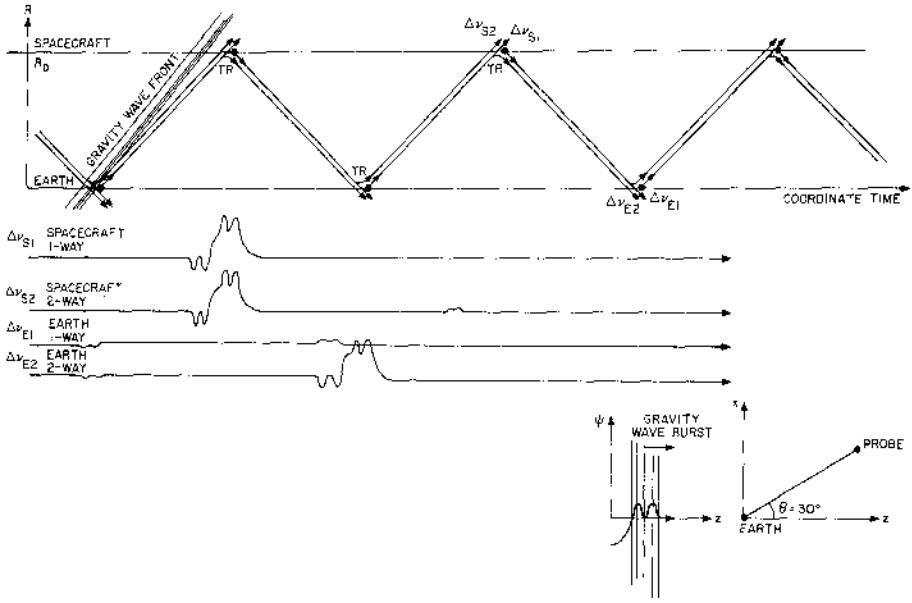


Fig. 12. Illustration of gravity-wave signature for a four-link correlated system, $\theta = 30°$.

are assumed to be approximately 1% [37]. Also in this region is the speculative formation of more massive black holes (10–10^4 $M_\odot$) in globular clusters out to $r \sim 500$ Mpc.

We will concentrate on the low-frequency, long-wavelength sources with $\nu < 10^{-2}$ Hz, $\lambda_{GW} > 3 \times 10^6$ km. These are most likely to result from bursts from the formation of supermassive ($M > 10^5$ $M_\odot$) black holes in galactic nuclei and quasars [11, 38]. Let us consider in more detail where such bursts might occur on Fig. 9. It seems that by the currently envisioned time-correlated Doppler signal approach described herein we can observe only those holes in the mass range $5 \times 10^5 < M < 10^7$ $M_\odot$. Presumably such holes form in the centers of galaxies very early. In fact, the quasars may be simply the first flow of gas onto newly formed holes [39, 40]. For this reason, to see the gravitational wave bursts from these black hole formations, we must look out at least to a redshift of approximately 2 or 3. Our values for the amplitude and event rate will therefore depend on the Hubble constant H_0 and the deceleration parameter q_0. We use a high-density universe with $H_0 = 100$ km sec^{-1} Mpc^{-1} and $q_0 = 1$.

Once this distance is chosen, we have set the amplitude of the resulting burst at earth for a given black hole of mass M, radiating with efficiency η, as is shown in Fig. 9. These levels are calculated following Thorne and Braginsky's work [11], as modified by Epstein and Clark [25], and shown plotted for efficiencies of 1% and 20%. The latter number seems the likely efficiency [41, 42] if galac-

tic core collapse results in a spiral collision of two black holes [38, 43]. We are encouraged to note that the sensitivity of our proposed mission overlaps the expected burst strength in part of our frequency window.

However, to observe such a burst, Nature must provide us a sufficient rate of events, here taken to be more than one burst per year. As Thorne and Braginsky [11] argue, looking out over the whole observable universe to $z < 3$, this event rate is proportional to $N\phi$, where N is the number of burst events each galactic nuclei suffers in its lifetime, and ϕ is the current number density per cubic gigaparsec of dead black holes. With the high-density universe, we require that $N\phi > 6 \times 10^7$ Gpc^{-3}, and for the currently popular low-density universe where $H_0 = 60$, $q_0 = 0.05$, we find that $N\phi > 5 \times 10^6$ Gpc^{-3} for there to be one event per year. Using Blandford's 1979 tabulation [40] of ϕ as a function of galactic type (assuming the dead holes are in galactic nuclei), we see that only the field galaxies having approximately our galaxy's luminosity ($L_{\text{gal}} \sim 5 \times 10^{36}$ W) are numerous enough ($\phi \geqslant 10^7$ Gpc^{-3}) to produce events at the required rate of at least one per year. Radio galaxies and giant elliptical galaxies are too rare [40] for their bursts to be seen with reasonable probability, even though they may have very massive black holes in their centers [44].

Thus the question of event rate can be rephrased, "Does a typical spiral galaxy like ours or Andromeda (M 31) have a black hole at its center?" Three years ago new evidence came to bear on this question. Using high-resolution infrared measurements, Lacy *et al.* [45] showed that our galaxy has $\sim 8 \times 10^6\ M_\odot$ of matter in the central half-parsec. Rodriguez and Chaisson [46] combined this with radio observations to propose a model with a $5 \times 10^6\ M_\odot$ central mass point in addition to the normal galactic center stellar population of $< 3 \times 10^6\ M_\odot$. If this "nonstellar central mass point" is a black hole accreting gas at $\sim 10^{-6}\ M_\odot$ yr^{-1}, it could explain many of the infrared features of the galactic center [47].

In 1979, M31 was imaged in the x-ray by the Einstein Observatory [48]. It was found that there is a point source in the nucleus with an x-ray luminosity of $L_x \sim 10^{38}$ erg^{-1}, a thousand times brighter than our galactic nucleus. It appears that a thermal source of x rays, such as accretion of gas onto a massive object, may be responsible. If so, M 31 would be intermediate between our galaxy and weak Seyfert galaxies such as NGC 4151 ($L_x \sim 3 \times 10^{43}$ erg^{-1}). The latter object has recently been argued [49] to have a central black hole of $\sim 4 \times 10^6\ M_\odot$. Presumably the difference in x-ray luminosity between these galactic nuclei is a function of the gas accretion rate.

More detailed observations are needed to tie down the galactic center black hole hypothesis. But we note that if it is correct and if our galaxy or M 31 are typical field galaxies, then a black hole of 10^6–$10^7\ M_\odot$ in such galaxies would radiate on formation in exactly the region of the gravitational wave spectrum we can search with best sensitivity. Thus, our search window appears to coincide with the highest probability region for supermassive black hole bursts. An alter-

native form of black hole burst will be from the coalescence of these black holes during the merger of galaxies.

§ (5): *Gravitational Aspects of Previous Space Missions and the Presently Proposed Mission Profile*

Experimental relativity and gravitation is a new departure in science and, thus far, gravitational space experimentation has tended to be a by-product of space missions with other primary goals. For example, the Doppler data obtained from the NASA Mariner and Viking missions have provided excellent results in the measurement of the gravitational time delay, the "fourth" test of general relativity discovered by I. I. Shapiro [8]. In the Introduction to this paper we have alluded to the possibility of repeating these tests at the appropriate time in the proposed mission. The search for gravitational radiation using Doppler techniques proposed in 1967 by Braginsky and Gertsenshtein [50] and by Anderson [51] in 1971 has made use of the normally acquired Doppler data and has prompted considerable rethinking in the technology for two-way tracking of the hopefully forthcoming International Solar Polar and Galileo missions [32]. To date only the 1976 GPA experiment has had as its primary goal the measurement of relativistic gravitational effects. We believe that the mission we now discuss is the logical sequel. Its objectives totally involve the study of gravitation; it relies on available technology and has a projected sensitivity adequate to observe the currently expected levels of pulsed radiation. The improved measurement of the gravitational red shift and second-order Doppler effect to be made during the first phase of the mission itself will make a solid contribution to our state of knowledge at a level significant to gravity theories. This, in fact, is a test of the internal self-consistency of the general theory of relativity in that it separately measures both the red shift and the time dilation effects. In our opinion experimental gravitation requires such a high level of commitment to measuring gravitational effects.

The two primary experiments, the red-shift measurement and the gravitational wave search, use the same basic equipment, but they require rather different orbital conditions. For the gravitational red-shift measurement, an orbit that carries the spacecraft in and out of a substantial fraction of the gravitational potential of the earth is needed. This would be satisfied by first placing the spacecraft in a highly eccentric earth orbit, where it would remain long enough to collect sufficient data for the red-shift experiment and, at the same time, to test the system for the ensuing search for gravitational waves. For the gravitational radiation search, an interplanetary orbit is required so that the light travel time from the spacecraft to the earth is a few times greater than the characteristic duration or period of the gravitation radiation signal to be detected.

Fortunately, the Space Transportation System now under development by NASA, consisting of the Shuttle and auxiliary propulsion units, allows these orbits to be achieved sequentially with reasonable ease and even permits recovery from earth orbit if required. The spacecraft would be equipped with two auxiliary rocket motors and lifted into space onboard the Shuttle. The first motor would be used to put the spacecraft into a highly eccentric earth orbit. After completion of the red-shift measurements, the second motor would be used to inject the spacecraft into an interplanetary orbit.

The principal criteria for selection of the eccentric earth orbit are maximum variation of the gravity potential and continuous or nearly continuous visibility of the probe from the ground station. Figure 13 shows the relationship between red-shift magnitude and eccentricity of a geosynchronous orbit [6]. The choice of the eccentricity parameter is governed by the requirements for maximum (ideally, continuous) communication time with the space probe and having elevation angles from the ground station greater than some minimum. Figure 14 shows the elevation angles for an equatorial tracking station and for a station at latitudes 35°. The orbital parameters used in the elevation angle calculations are listed in Table IV. A somewhat higher eccentricity, about 0.6, may be acceptable depending on station location.

During the earth-orbit phase of the mission, when signal strength is not a problem, the red-shift experiment could be run from a station with relatively small antenna size and low transmitter power located closer to the equator. For the interplanetary orbit phase of the mission a D.S.N. deep-space tracking station will be required because of the low signal level resulting from the large dis-

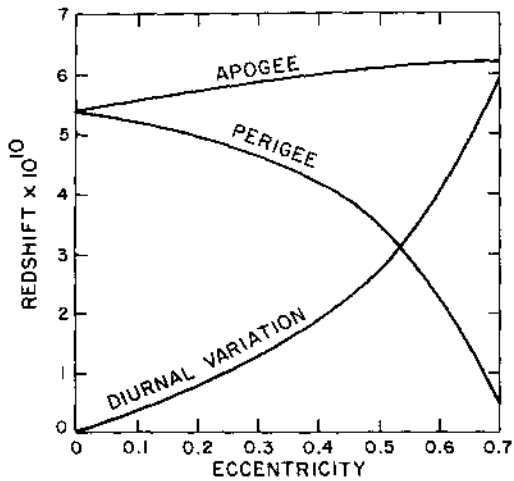


Fig. 13. Red-shift magnitude vs. eccentricity of 24-hr geocentric orbit.

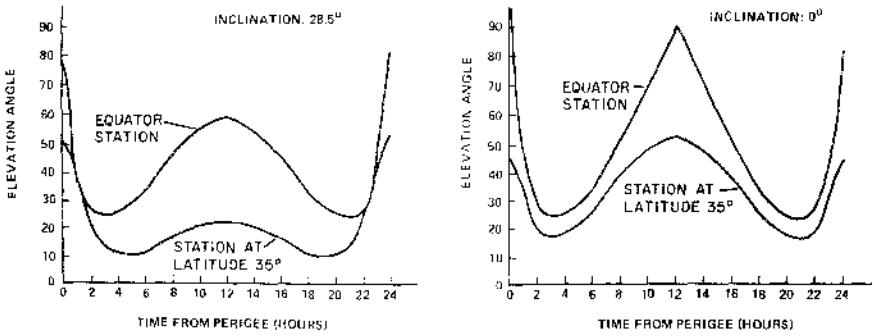


Fig. 14. Elevation angles for 24-hr orbits at inclinations of 28.5° and 0°.

Table IV. Earth Orbit Characteristics

Period	24 hr
Eccentricity	0.5
Inclination	0°
Semimajor axis	4.22×10^7 km
Range at perigee	1.47×10^4
Range at apogee	5.69×10^4
Velocity at perigee	5.32×10^3 km sec^{-1}
Velocity at apogee	1.77×10^3 km sec^{-1}

tance to the spacecraft. A substantial commitment of observing time is required—at least 8 hr per day and nearly continuous coverage by additional stations is very desirable in view of the low estimated event rate.

The criteria for selection of the interplanetary orbit are not critical. The inclination of the interplanetary orbit relative to the ecliptic plane should be rather small, and the maximum distance of the space probe from the earth should reach at least 6 AU [see equation (6)]. During the time of maximum separation between earth and space probe, the sun, earth, and probe should not be in line in order to prevent solar microwave noise from entering either the earth or spacecraft receiver systems.

§ (6): *Conclusions*

Experiments to test theories of gravitation are so demanding that each new experiment capable of achievement joins a short, prestigious list. Therefore, it is noteworthy when a single spacecraft mission promises to allow the performance of two (or possibly more) such experiments, including a search for gravitational radiation. This circumstance has the consequence that a number of

investigators and institutions potentially can participate in preparation, execution, and interpretation of the mission.

The key new element we proposed herein is the addition of a highly stable hydrogen maser clock onboard the spacecraft so that we can have four links and, by use of time correlation, substantially increase the amount of information in the data to allow the separation of gravitational red-shift and second-order Doppler effects. The additional links of radio data provides additional signatures of a gravitational wave burst and increases substantially our confidence in the removal of spurious signatures. This allows a Doppler signal fluctuation to be unambiguously identified as a gravitational wave if the burst is of sufficient strength. We showed in detail how the minimum detectable strength depends on the clock stability. It appears that with hydrogen maser clocks available in the next decade we should be able to detect gravitational wave bursts emitted by supermassive black holes forming or colliding anywhere in the observable universe ($z \lesssim 3$).

Another advantage of this high clock stability is that it allows very sensitive measurements of the gravitational red shift and the second-order Doppler effect. By placing the clock in orbit, we should be able to improve the previous suborbital test by a factor of 30. At this level of $\sim 5 \times 10^{-6}$, the red-shift experiment will break new experimental ground on tests of the internal self-consistency of general relativity—the meshing of the equivalence principle, the special theory of relativity, and the isotropicity of the velocity of light. These are the cornerstones of all theories of gravity.

The envisioned mission further has the remarkable feature that the same equipment is used for the two primary investigations as well as for possible supplementary investigations. The instrumentation is a natural evolution of that flown successfully on the Gravity Probe A Redshift Experiment in 1976. These facts are important to the economic practicality of the mission. Once developed and proved in this flight, duplicate counterparts of the equipment can be incorporated in other spacecraft to continue these and related lines of inquiry. The expectation that one or more gravitational waves could be detected during the course of the envisioned mission has been argued on source assumptions that seem reasonable at this time.

Admittedly, the search for gravitational radiation cannot be completely assured of success within the current state of knowledge of sources of this radiation. This uncertainty should be viewed against the great significance of a positive detection of a gravitational wave or a definitive null result at a level for which detection is theoretically predicted. Further, this recognized risk is balanced by the ensured success of the red-shift experiment. Naturally, much effort is still needed to refine and optimize the proposed gravity mission, presented here in conceptual outlines. Its broad features are nonetheless clear and of such attractiveness that the required effort is strongly justified.

Acknowledgments

We gratefully acknowledge useful and interesting discussions with our many colleagues who have influenced the development of this article. In particular we would like to thank J. D. Anderson, E. M. Blomberg, L. S. Cutler, R. W. P. Drever, R. W. Davis, P. B. Eby, F. B. Estabrook, B. F. Farrell, G. B. Field, R. W. Hellings, M. W. Levine, A. P. Lightman, A. Liu, E. M. Mattison, W. T. Ni, W. H. Press, N. G. Roman, H. D. Wahlquist, G. C. Weiffenbach, and R. S. Wolff. This work was supported, in part, by the National Science Foundation, Harvard's Society of Fellows, the National Aeronautics and Space Administration, the Smithsonian Institution, and the Revson Foundation.

References

1. Vessot, R. F. C., and Levine, M. W. (1978b). In *A Close Up of the Sun*, M. Neugebauer and R. W. Davis, eds., JPL Publication, pp. 457–497.
2. Vessot, R. F. C. (1979). *Radio Sci.*, **14**, 629–647.
3. Ni, W. T. (1977). *Phys. Rev. Lett.*, **38**, 301.
4. Ni, W. T. (1979). Preprint.
5. Vessot, R. F. C., and Levine, M. W. (1978a). *Gen. Rel. Grav.*, **20**, 181. Also in *Experimental Gravitation, Proceedings of the Accademia Lincei*, Vol. 34, pp. 371–391.
6. Kleppner, D., Vessot, R. F. C., and Ramsey, N. F. (1970). *Astrophys. Space Sci.*, **6**, 13–32.
7. Vessot, R. F. C., and Levine, M. W. (1971). In *Proceedings of the Conference on Experimental Theories*, R. W. Davis, ed. California Institute of Technology, pp. 54–64.
8. Shapiro, I. I. (1979). In *Einstein Memorial Volume*, A. Held, ed., Plenum Press, New York.
9. Will, C. M. (1979). In *General Relativity. An Einstein Centenary Volume*, S. W. Hawking and W. Israël, eds., Cambridge U. P., Cambridge, pp. 24–89.
10. Taylor, J. H., Fowler, L. A., and McCulloch, P. N. (1979). *Nature*, **277**, 437.
11. Thorne, K. S., and Braginsky, V. B. (1976). *Astrophys. J. Lett.*, **204**, L1.
12. Estabrook, F. B., and Wahlquist, H. D. (1975). *Gen. Rel. Grav.*, **6**, 439.
13. Vessot, R. F. C., and Levine, M. W. (1974). In *Proceedings of the 28th Annual Symposium on Frequency Control* (U.S. Army Electronics Command, Ft. Monmouth, New Jersey), pp. 408–414.
14. Armstrong, J. W., Woo, R., and Estabrook, F. B. (1979). *Astrophys. J.*, **230**, 570.
15. Brecher, K. (1977). *Phys. Rev. Lett.*, **39**, 1051, 1236; Newman, D., Ford, G. W., Rich, A., and Sweetman, E. (19). *Phys. Rev. Lett.*, **40**, 1355.
16. Will, C. M. (1974). *Phys. Rev. D*, **10**, 2330.
17. Thorne, K. S., Lee, D. L., and Lightman, A. P. (1973). *Phys. Rev. D*, **7**, 3564.
18. Lightman, A. P., and Lee, D. L. (1973). *Phys. Rev. D*, **8**, 364.
19. Haugan, M. P., and Will, C. M. (1977). *Phys. Rev. D*, **15**, 2711.
20. Vessot, R. F. C. (1981). In *Proceedings of the International Symposium on Time and Frequency*. Natural Physical Laboratory, New Delhi, India (February 10–12, 1981).
21. Vessot, R. F. C., Levine, M. W., Mattison, E. M., Blomberg, E. L., Hoffman, T. E., Nystrom, G. U., Farrel, B. F., Decher, R., Eby, P. B., Baugher, C. R., Watts, J. W., Teuber, D. L., and Wills, F. D. (1980). *Phys. Rev. Lett.*, **45**, 2081.
22. Allan, D. W. (1966). *Proc. IEEE*, **54**, 221. *J. Inst. Electron. Telecommunication Eng.*, in press.

23. Vessot, R. F. C., and Levine, M. W. (1979). NASA Experimental Final Redshift Report, GPA Project Report, Contract NAS 8-27969.
24. Vessot, R. F. C., Mattison, E. M., and Blomberg, E. L. (1979). In *Proceedings of the 33rd Annual Frequency Control Symposium* (USAERADCOM, Ft. Monmouth, New Jersey), pp. 511–514.
25. Epstein, R., and Clark, J. P. A. (1979). In *Sources of Gravitational Radiation*, L. L. Smarr, ed., Cambridge U. P., Cambridge.
26. Weiss, R. (1979). In *Sources of Gravitational Radiation*, L. L. Smarr, ed., Cambridge U. P., Cambridge.
27. Bertotti, B. (1973). *Astrophys. Lett.*, **14**, 51; Rosi, L. A., and Zimmerman, R. L. (1976). *Astrophys. Space Sci.*, **45**, 447; Anderson, A. J. (1977). In *Gravitazione Sperimentale*, ed. B. Bertotti, Proceedings of the International Symposium on Experimental Gravitation, Pavia, Italy, 17–20 September, 1976, Accademia Nazionale dei Lincei, Roma; Hellings, R. W. (1979). J. P. L. preprint; Carr, B. J., Cal. Tech preprint OAP-566; Bertotti, B. and Carr, B. J., Cal. Tech. preprint OAP-564; Mashhoon, B., and Grishchuk, L. P., Cal. Tech. preprint OAP-562; Turner, M. S., Enrico Fermi Institute preprint 79-22.
28. Thorne, K. S. (1978). In *Theoretical Principles in Astrophysics and Relativity*, University of Chicago Press, Chicago.
29. Drever, P., private communication, gave important input to the adaptation process.
30. Thorne, K. S., Caves, C. M., Sandberg, V. D., Zimmermann, M., and Drever, R. W. P. (1979). In *Sources of Gravitational Radiation*, L. L. Smarr, ed., Cambridge U. P., Cambridge.
31. Piran, T., Reiter, E., Unruh, W., and Vessot, R. F. C. (1981). To be published.
32. Estabrook, F. B., Hellings, R. W., Wahlquist, H. D., and Wolff, R. S. (1979). In *Sources of Gravitational Radiation*, L. L. Smarr, ed., Cambridge University Press, Cambridge. See also: Estabrook, F. B., and Wahlquist, H. D. (1978). *Acta Astron.*, **5**, 5; Wahlquist, H. D., Anderson, J. D., Estabrook, F. B., and Thorne, K. S. (1977). In *Gravitazione Sperimentale, Atti dei Convegni Lincei*, B. Bertotti, ed., **34**, 335; Anderson, J. D., and Estabrook, F. B. (1979). *J. Spacecraft Rockets*, in press; F. B. Estabrook (1978). In *A Close-Up of the Sun*, J. P. L. Publication 78-70, M. Neugebauer and R. W. Davis, eds.
33. Mashhoon, B. (1979). *Astrophys. J.*, **227**, 1019; Turner, M. S. (1979). Enrico Fermi preprint 79-22.
34. Kaufmann, W. J. (1970). *Nature*, **227**, 157.
35. Hellings, R. W., Callahan, P. S., Anderson, J. D., and Moffet, A. T. (1981). *Phys. Rev. D*, **23**, 844.
36. Zimmerman, M. and Thorne, K. S. (1978). Cal. Tech. preprint.
37. Shapiro, S. L. (1979). In *Sources of Gravitational Radiation*, L. L. Smarr, ed., Cambridge U. P., Cambridge.
38. Rees, M. (1977). In *Gravitazione Sperimentale Atti de Convegni Lincei*, B. Bertotti, ed.
39. Rees, M. J. (1977). *Ann. N.Y. Acad. Sci.*, **302**, 613.
40. Blandford, R. (1979). In *Sources of Gravitational Radiation*, L. L. Smarr, ed., Cambridge U. P., Cambridge.
41. Smarr, L. L. (1979). In *Sources of Gravitational Radiation*, L. L. Smarr, ed., Cambridge U. P., Cambridge.
42. Detweiler, S. L. (1979). In *Sources of Gravitational Radiation*, L. L. Smarr, ed., Cambridge U. P., Cambridge.
43. Fowler, W. A. (1964). *Rev. Mod. Phys.*, **36**, 545.
44. Sargent, W. L., Young, P. J., Boksenberg, A., Shortridge, K., Lynds, C. R., and Hartwick, F. D. A. (1978). *Astrophys. J.*, **221**, 731; Young, P. J., Westphal, J. A., Kristian, J., Wilson, C. P., and Landaver, F. P. (1978). *Ibid.*, **221**, 721; de Vaucouleurs, G., and Nieto, J. L. (1979). *Ibid.*, **230**, 697; Young, P. J., Sargent, W. L. W., Kristian, J., and Westphal, J. A. (1979). *Ibid. Ap. J.*, **234**, 76.
45. Lacy, J. H., Haas, F., Townes, C. H., and Geballe, T. R. (1979). *Astrophys. J. (Lett.)*, **227**, L17; Wollman, E. R., Geballe, T. R., Lacy, J. H., Townes, C. H., and Rank, D. M. (1976). *Astrophys. J. (Lett.)*, **218**, L103.

46. Rodriguez, L., and Chaisson, E. J. (1979). *Astrophys. J.*, **228**, 734.
47. Lynden-Bell, D., and Rees, M. J. (1979). *Mon. Not. R. Astron. Soc.*, **152**, 461.
48. Van Speybroeck, L., Epstein, A., Forman, W., Giacconi, R., Jones, C., Liller, W., and Smarr, L. (1979). *Astrophys. J. (Lett.)*, Nov. 15.
49. Lightman, A. P., Giacconi, R., and Tananbaum, H. (1978). *Astrophys. J.*, **224**, 375.
50. Braginsky, V. B., and Gertsenshtein, M. E. (1967). *JETP Lett.*, **5**, 287.
51. Anderson, A. J. (1971). *Nature*, **229**, 547.